International Journal of Heat and Mass Transfer 213 (2023) 124340

Contents lists available at ScienceDirect

International Journal of Heat and Mass Transfer

journal homepage: www.elsevier.com/locate/hmt

Designing air handling unit in data center and estimating its performance

Zixing Wang, Hao Ding, Le Lei, Nan Li, Wenquan Tao*

Key Laboratory of Thermo-Fluid Science & Engineering of MOE, Xi'an Jiaotong University, Xi'an, Shaanxi 710049, PR China

ARTICLE INFO

Article history:
Received 17 March 2023
Revised 14 May 2023
Accepted 23 May 2023
Available online 3 June 2023

Keywords:
Data center
Air handling unit
Turbulent flow
Dimple/protrusion channel
Heat transfer enhancement

ABSTRACT

In this paper, the construction process of the enhanced plate, the heat transfer and fluid flow characteristics, and the domain decomposition method for AHU performance estimation are presented. The AHU heat exchanger 3D model is built from plate modeling to heat exchanger assembling. The heat transfer plate modeling starts from a basic flat plate, elliptic cylindrical dimples (ECDs) are firstly added to the fixed location, and then spherical crown dimples (SCDs) are applied to the flat surface among the ECDs. For the enhanced channels, the effect of channel height is weaker than SCD depth on the Nusselt number and friction factors. For all enhanced channels, the PECs are larger than 1.1 within Re from 5000 to 35,355. The performance of a deeper depth of SCD is superior to that of a shallow one when the channel height is the same. Among the nine channels studied, the highest enhanced effects are obtained for "H12-R10-h4" (PEC=1.45 at Re=5000). And all nine enhanced channels can enhance heat transfer at the same pressure drop among the Reynolds number of 5000 to 35,355. The energy saving performance decreases with Re, and the channels with smaller SCD depth can save more energy when channel height is identical at the higher Reynolds number region. A decomposition thermal design method is proposed for the cross-flow AHU heat exchanger design, and the typical AHU design result is picked based on the heat exchange rate and flow loss power. The recommended heat exchanger is "H7.5-R10-h3" whose heat exchange rate is 40.5 kW when flow loss power is 3.25 kW.

1. Introduction

Air handling units (AHU) are widely used in modern data center for cooling the air which has been heated by the IT devices in data center. The AHU heat exchanger can work under the water evaporation-assisted mode [1–10]. As the first phase of our study here we only investigate the AHU performance under dry conditions which also serves as the fundamentals for the water-assisted mode. The AHU heat exchanger is a typical multi-channel thin-plate heat exchanger for air-to-air heat transfer. These heat transfer thin plates are usually made from the same molds, and two adjacent plates are arranged staggered at 90° angle. Many such staggered-arranged plates form one AHU heat exchanger. Fig. 1 is a sample of the AHU heat exchanger assembled by many plates.

The key part of the AHU heat exchanger design is the geometry design of the heat transfer plates. Since the convective heat transfer in a channel with smooth plates is quite weak, special enhancement technologies must be taken for the plates. Once the plate design is done, the geometry model of the whole heat exchanger can be built. The heat transfer plate of an AHU has three main characteristics: 1. The plate is thin; 2. The hot air and cold air are separated by the plates and flow in their respective channel with limited height. 3. The hot and cold air should be kept clean in operation. Due to those characteristics, some passive heat transfer enhancement methods, such as inserts, nanofluids [11], etc. cannot be applied. Dimples are an appropriate technology to be adopted in the plates due to their advantages in heat transfer enhancement, small pressure drop, and simple fabrication. The structure of dimple/protrusion surfaces has been extensively studied in the past few decades [12–26]. In this study, the ECD and SCD are both adopted on the two sides of the heat transfer plate to enhance heat transfer. The ECDs are placed on the fixed location of one side of the plates and the SCDs are placed among the locations of ECD. In this paper, the heat transfer enhancement performance of the proposed SCD and ECD enhanced flow channels is discussed. And finally, a decomposition method of the thermal design (DMTD) is proposed to calculate the total heat transfer rate of the whole AHU heat exchanger.

* Corresponding author.
E-mail address: wqtao@mail.xjtu.edu.cn (W. Tao).

https://doi.org/10.1016/j.ijheatmasstransfer.2023.124340
0017-9310/

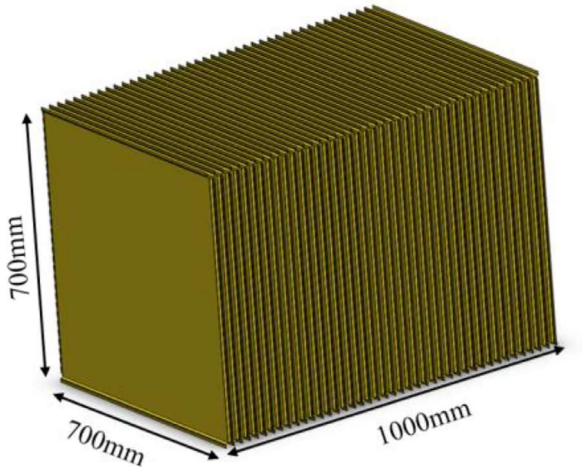

Fig. 1. The simple heat exchanger 3D model.

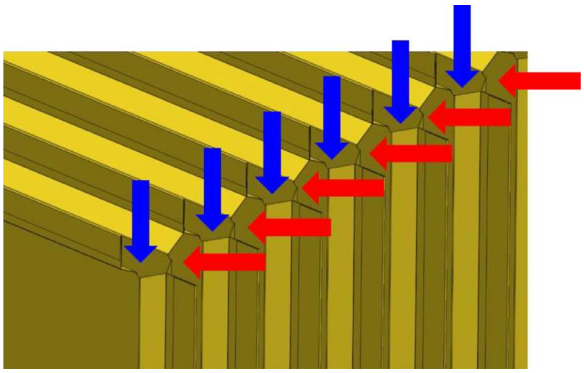

Fig. 2. The cross-flow direction of two inlet air streams.

In the following, the construction process of the enhanced plate is first presented, then the heat transfer and fluid flow characteristics are discussed in detail. Performance comparison is conducted for the nine enhanced channels from three constraints. Then for the design of an AHU heat exchanger, the DMTD is proposed to avoid the inconvenience of determining the correction factor Ψ of the log-mean temperature difference of the cross flow. And this method is used to design a typical AHU heat exchanger. Finally, some conclusions are drawn.

2. Reconstruction of the air handling unit heat exchanger

2.1. The AHU geometry parameters restrictions of this study

To reconstruct an AHU heat exchanger, it is necessary to give some geometry parameter restrictions. The restrictions based on some engineering practices applied in this paper are as follows: 1. the heat exchanger size does not exceed: 700mm*700mm*1000 mm; 2. the plate thickness is 0.15 mm.

The 3D outline configuration is built with the above restrictions in Fig. 1. The heat exchanger plates have bent edges that can meet the plates' assembling requirements. Fig. 2 is the enlarged view of one corner of the heat exchanger, in which the blue and red arrows show the cold air flow direction and the hot air flow direction, respectively. The flow pattern of the two air streams is the typical cross-flow in the heat exchanger. Fig. 3 shows the basic flat plate used for the heat exchanger assemblage in Fig. 1, the width and length are both 700 mm, and the four edges of the plate are bent.

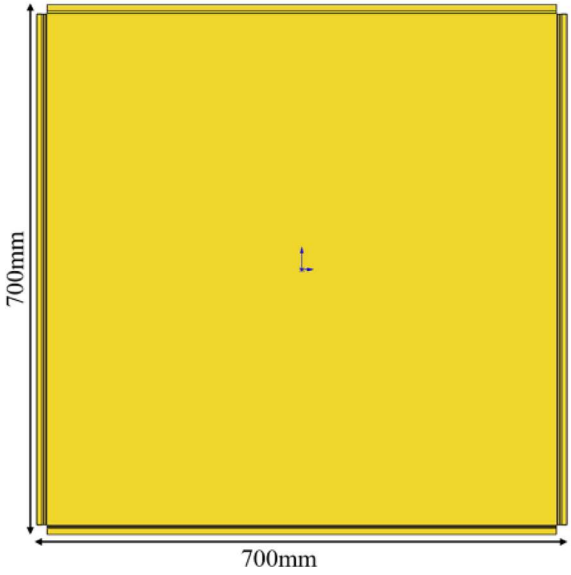

Fig. 3. Top view of the basic flat plate.

2.2. The heat transfer enhancement structure design and modeling

The basic flat plate is like a blank canvas, and we can add appropriate heat transfer enhancement structure on it just like painting. Fig. 4 shows the "painting" process.

First of all, some ECDs are added to the fixed location of the basic flat plate. Fig. 4(a) shows the top view of the plate, which is named the elliptic cylindrical supporting enhanced plate. Fig. 4(b) shows the up and down side view of the plate, the upside of the plate is a dimpled surface and the downside of the plate is a corresponding protrusion surface. 81 ECDs are applied with a 9×9 pattern. The distances between adjacent dimples along the width and length direction are both 70 mm. And the center of these array-centered ECD is also the center of the flat plane. With the arrangement, the elliptic cylindrical supporting enhanced plate is still centrosymmetric. A pictorial view of the ECD is shown in Fig. 4(c), the long axis of the ellipse is 16 mm, the short axis is 4 mm, and the cylinder height is 12 mm. The long axis length and short axis length are fixed in this work, but the ECD height has different values. After the ECD modeling on the plate, many SCD are added to the flat area among the ECD. Fig. 4(d) shows an example of the top view of the SCD enhanced plate where the small elliptic circles between the SCD circles show the location of the ECD at the plate.

Fig. 5 shows the detailed AHU heat exchanger reconstruction process based on the enhanced plates shown in Fig. 4(d). To make the process more intuitive, the heat exchanger shown in Fig. 5 only consists of three plates and two air flow channels. As shown in Fig. 5(a), the central plate is unrotated but the upper and lower plates are both rotated by 90°. After rotation, the two rotated plates are assembled to the unrotated plate along their assembling direction. Fig. 5(b) shows the assembled heat exchanger of three plates, the two adjacent plates form the air flow channels for hot air and cold air. For large heat exchangers consisting of many plates, the reconstruction process is the same.

Different geometry parameters of the ECD and the SCD have been modeled. Apart from the fixed lengths of the ECD's two axes, the SCD spherical radius is constant (10 mm). The effects of SCD dimple depth (2 mm, 3 mm, and 4 mm) and ECD height (7.5 mm, 10 mm, and 12 mm) have been studied. For the convenience of presentation, each plate pattern is named as follows: "Hx-Rx-hx", in which "H" represents channel height, "R" represents spherical

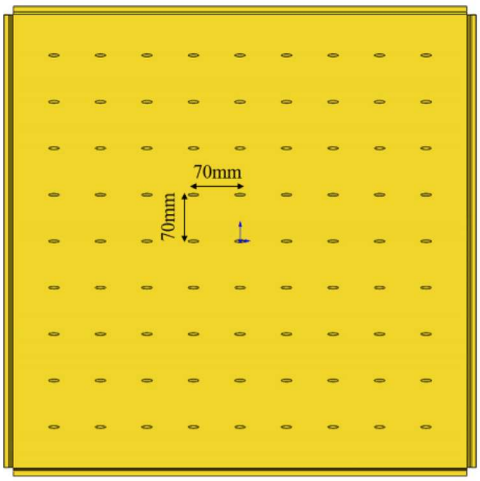

(a) Top view of the ECD enhanced plate

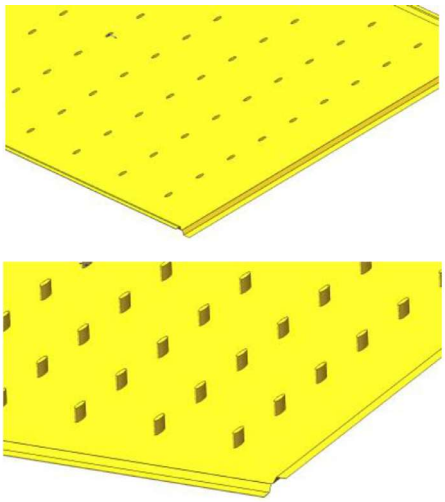

(b) 3D views of the up and down side of the ECD enhanced plate

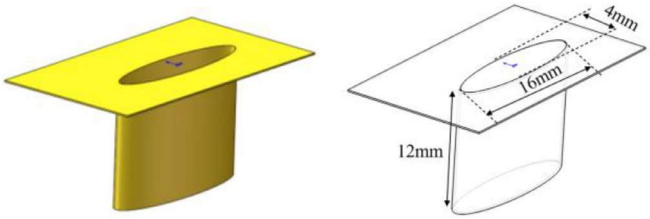

(c) The ECD

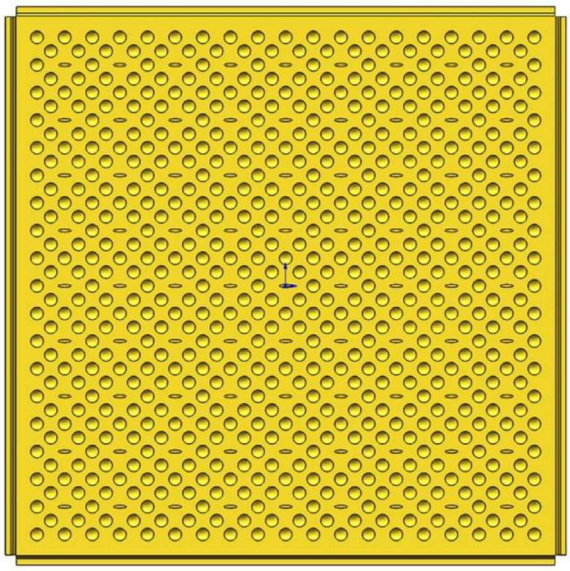

(d) Top view of SCD enhanced plate[1]

Fig. 4. The ECD and SCD enhanced plate.

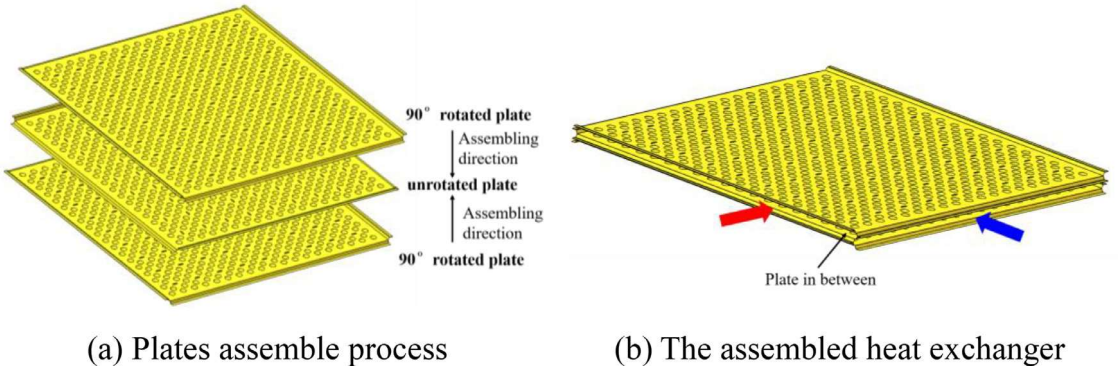

Fig. 5. Example of the AHU heat exchanger reconstruction process.

radius, "h" represents spherical dimple crown depth, and "x" refers to the individual values in mm.

3. Heat transfer and fluid flow performance of enhanced channels

To evaluate the thermo-hydraulic performance of the proposed dimple/protrusion enhanced channels, the performance evaluation plot method proposed by Fan et al. [27] is used. The heat transfer enhancement ratio for identical pumping power is often named the performance evaluation criterion (*PEC*) and is calculated by:

$$PEC = \frac{Nu/Nu_0}{(f/f_0)^{1/3}} \quad (1)$$

where Nu_0 and f_0 are the Nusselt number and friction factor of the corresponding flat plate channel, which is regarded as the reference structure. In the following, the effects of ECD height and SCD depth on heat transfer, friction factor, and *PEC* are discussed.

3.1. Effect of ECD and SCD on Nusselt number

For the convenience of discussion when the effect of one parameter is studied, the other parameter is kept the same. ECD height is the channel height between two adjacent plates. Once the ECD height is fixed, different SCD depth means the different surface structures of the dimple wall side and protrusion wall side. A comprehensive comparison of the numerical results is presented in Fig. 6, where the characteristic lengths of the Reynolds number and Nusselt number are the hydraulic diameter. In the figure, the three ECD heights are named: the "H12" series, the "H10" series, and the "H7.5″ series respectively, and the three SCD depths are named: "h2" series, "h3" series, and "h4" series respectively. The compared Reynold number range is from 5×10^3 to 3.53×10^4. For the convenience of comparison, the numerical results of the reference cases are also presented. The total variation characteristics of *Nu* can be summarized as follows. First, the Nusselt number increases with the Reynolds number, and the increasing curve slope of the three enhanced channels is appreciably larger than the referenced channel. Second, the Nusselt number increases appreciably with SCD, caused by the enhanced fluid mixing and increased velocity gradient near the wall. Third, the Nusselt number increases with ECD height slightly, showing that the effect of "H" on the heat transfer is weaker than "h".

3.2. Effect of ECD and SCD on friction factor

In Fig. 7. the predicted friction factors of the nine enhanced channels are provided. Fig. 7(a), Fig. 7(b), and Fig. 7(c) show the effect of the depth of the SCD, and Fig. 7(d), Fig. 7(e), and Fig. 7(f) present the effect of channel height (depth of ECD). It can be seen that the friction factors of the nine enhanced channels are appreciably higher than the corresponding plate channel, and the friction factors decrease with the increase in Re with a gradually becoming mild trend. The value of SCD strongly affects *f*: the larger the SCD the higher the *f*, which is consistent with the effect on the Nusselt number.

3.3. Effect of ECD and SCD on PEC

As shown in Figs. 6 and 7, both Nu and *f* of the nine enhanced channels increase with the depth increase of SCD, with the increase of friction factor being more significant. It is here the problem occurs: how about the comprehensive thermos-hydraulic performance of the enhanced channels? One important comparison criterion is whether the enhanced structure can enhance heat transfer under an identical pumping power. This performance comparison criterion is shown by Eq. (1). The reference cases used to calculate *PEC* are the corresponding flat plate cases with the same channel heights. The effects of "h" and "H" on *PEC* are presented in Figs. 8 and 9, respectively, with *Re* being the abscissa.

From Fig. 8, three features may be noted. First, it can be seen that for all the cases studied, *PEC*s are all larger than 1.1, indicating that for the nine enhanced channels, at the identical pumping power constraint, they can enhance at least 10% heat transfer rates. Second, there is a quite general trend: *PEC* versus Re performance is related to channel height "H" and SCD depth "h". When "h" = 4 mm, *PEC* for the bigger channel height case ("H=12 and H=10″) decreases with Re, but *PEC* of the smaller channel height case ("H=7.5″) firstly increases to a peak value and then starts to decrease, and it could be named as peak phenomenon. The *PEC* versus *Re* peak phenomenon occurs for the channels when the "h" decrease and "H" increase until the channel (H12-R10-h2) with the biggest "H" and smallest "h" in this study, whose *PEC* continuously increases with *Re*. The *PEC* peaks all occur at the smaller *Re* region (6000–10,000). The trend of *PEC* changes at the higher *Re* region gradually becomes mild. Third, the enhanced effect of SCD depth equal to 4 mm is the strongest, and the highest *PEC* reaches 1.45. The enhanced effects of "h" = 3 mm are larger than that of "h" = 2 mm.

When SCD depth is fixed, the geometry of the dimple and protrusion wall surface is fixed, then the decrease of ECD depth means the two wall surfaces become closer. From Fig. 9, it is clear that the channels with bigger channel heights have better heat transfer enhancement performance under identical pumping power. For the "h2" series channels, the channel height "H" greatly influences *PEC*. As Fig. 8(a) shows, when SCD depth is 2 mm, the *PEC* of the H12 channel increases with *Re*. But *PEC* starts to decrease at the high *Re* region when "H" decreases.

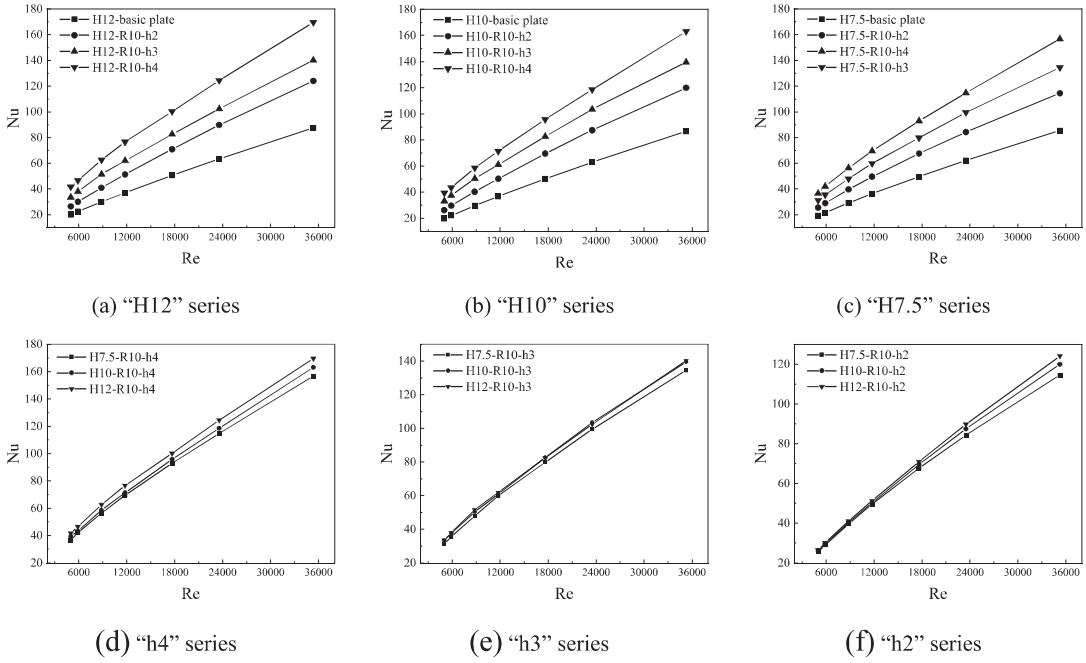

Fig. 6. *Nu* versus Reynolds number for nine types of enhanced flow channels.

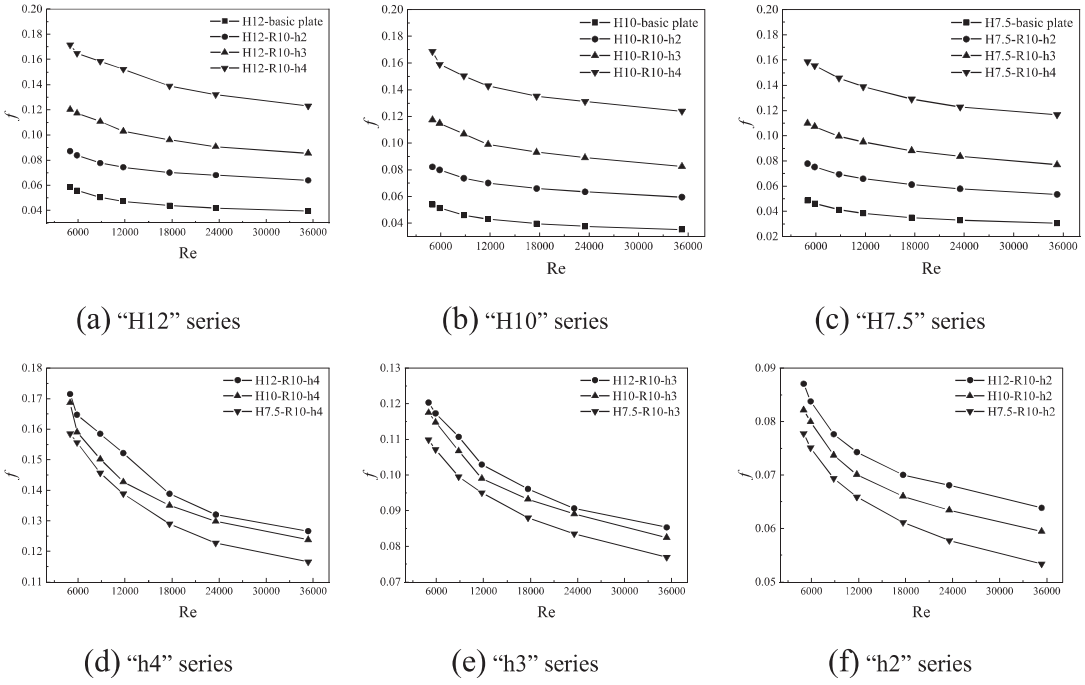

Fig. 7. *f* versus Reynolds number for nine types of enhanced flow channels.

For the "h3" series channels, *PEC*s versus *Re* all follow the peak phenomenon. For "h4" cases, the peak phenomenon occurs only for the "H12" channel, the *PEC*s continuously decrease with *Re* when "H" is as big as 10 mm and 12 mm.

In conclusion, the heat transfer enhancement performance at the low Reynold numbers range is higher than that at the high Reynolds number range; the performance of a deep depth of SCD is superior to that of a shallow one when channel height is the same; the performance of bigger channel height is superior to that of a smaller one when SCD depth is same. Among the nine channels studied, the highest enhanced effects are obtained for "H12-R10-h4" (*PEC*=1.45 at *Re*=5000), and the channel of "H7.5-R10-h2" has the lowest enhanced effects with the smallest of *PEC* being about 1.11 at *Re*=35,355.

3.4. Energy saving effectiveness performance comparison on the general evaluation plot

The discussion on *PEC* comparison shows the heat transfer enhancement rate between enhanced structure and reference structure with identical pumping power. For more general energy saving effectiveness of enhanced surface, the performance evaluation

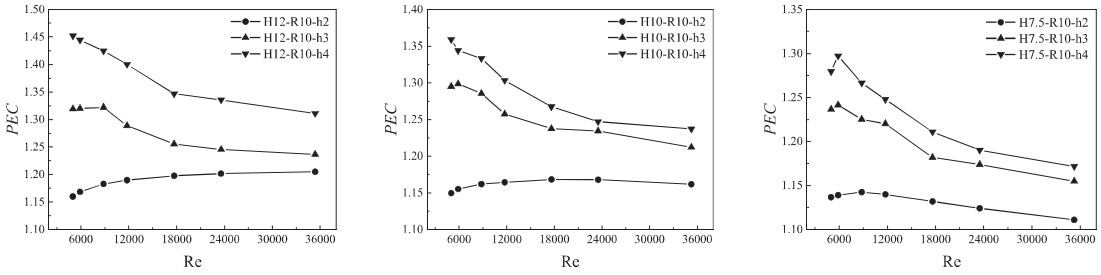

(a) "H12" series (b) "H10" series (c) "H7.5" series

Fig. 8. *PEC* versus *Re* number for three H-series.

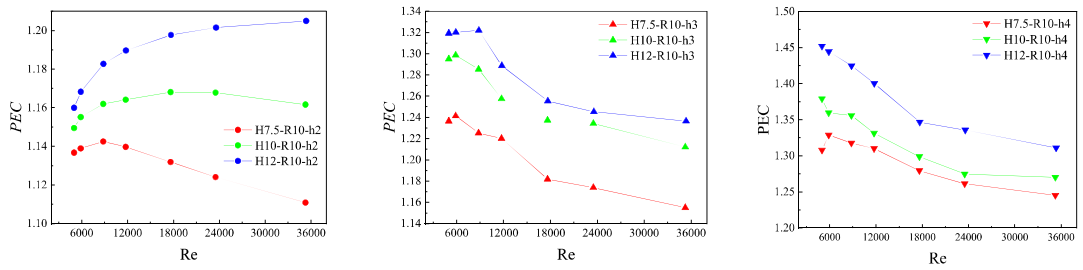

(a) "h2" series (b) "h3" series (c) "h4" series

Fig. 9. *PEC* versus *Re* number for three h-series.

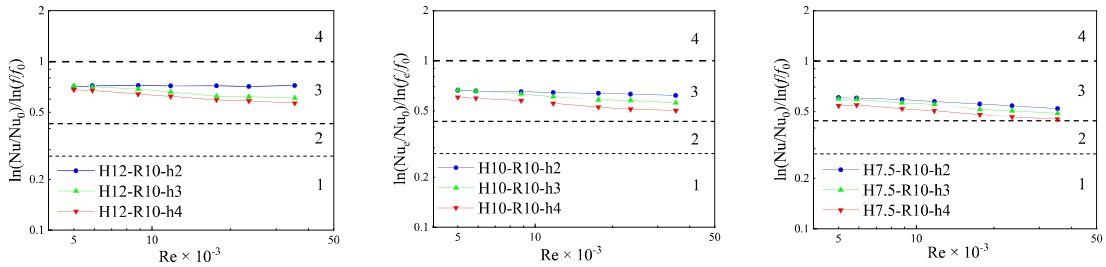

(a) "H12" series (a) "H10" series (a) "H7.5" series

Fig. 10. Performance evaluation plot for three "H" series.

method revised by Ji et.al. [28] is adopted for all night enhanced channels, in which the reference channels are the corresponding basic place channels with the same channel height. Fig. 10 shows the performance evaluation plot results for three "H" channel series. In the figure, there are four horizontal regions representing heat transfer enhancement (HTE): without energy saving: (1); HTE at identical pumping power: (2); HTE at identical pressure drop: (3) and HTE at the same flow rate: (4), respectively. The four regions represent different efficiency levels, and the higher the level the better the HTE technique. The values of the three dividing lines of the four levels depend on the practical reference structure. For the three H series, the "H12" series are 0.275, 0.429, and 1.0; the "H10" series are 0.277, 0.433, and 1.0; and the "H7.5″ series are 0.280, 0.440, and 1.0, respectively for the three dividing lines.

From Fig. 10, it is clear that all nine enhanced channels are in Level 3 among the studied Reynolds number region, which means all enhanced channels can enhance heat transfer at the same pressure drop. For most channels, the energy saving performance decreases with *Re*, and the decline rate increase with the "h" increase. As for the influence of SCD depth "h", the channel with smaller "h" can save more energy at the same height and Reynolds number.

4. Thermal design of AHU and heat transfer and pressure drop estimation

4.1. Thermal design of an AHU

The following assumptions are adopted in the thermal design of an AHU:1. An AHU has its repeated arrangement of hot and cold channels (see Fig. 2). Each pair of hot and cold channel have the same performance and one pair of hot-cold channel is selected as its representative; 2. The hot air channels and cold air channels are composed of the same centrosymmetric plates. And the area-averaged heat transfer coefficients of the entire channel presented above are used. 3. The volume flow rates of the hot and cold air are the same. 4. The reference temperature for air properties is based on the average one of the inlet temperature and outlet temperature; 5. The heat transfer loss to surroundings, and the thermal resistance of the plate and fouling are all neglected.

The hot and cold air streams are of the cross type, and when the logarithmic temperature difference method (LTDM) is used to determine the total heat transfer rate, a correction factor Ψ should be used to determine the temperature difference between hot and cold air streams [29]. The values of Ψ either expressed in discrete

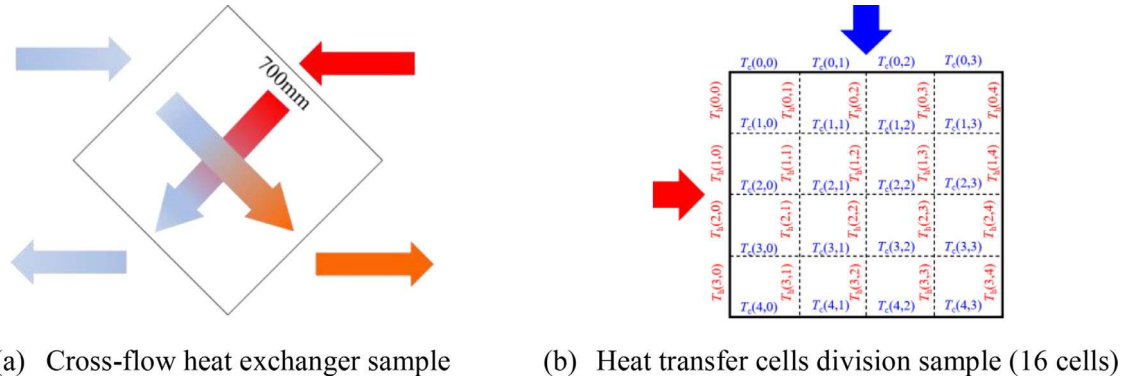

Fig. 11. Cross-flow heat exchanger sample and finite heat transfer cells division sample.

lines with the parameter of R (R=($T_{h,in}$-$T_{h,out}$)/($T_{c,out}$-$T_{c,in}$) and P (P=($T_{c,out}$-$T_{c,in}$)/($T_{h,in}$-$T_{c,in}$)) [29] or by Nusselt's infinite series solution [30]. Both the two methods are not convenient for engineering design.

On the other hand, the correction factor Ψ will approach 1 when P approaches zero. Especially, when P is less than 0.1, Ψ is about 0.99 [29]. For the whole AHU heat exchanger used in the data center, the difference between inlet hot air and inlet cold air is quite fixed, usually about 20 °C, if we divide the entire heat transfer area into enough number small cells, ($T_{c,out}$-$T_{c,in}$) will be pretty small compared with ($T_{h,in}$-$T_{c,in}$), and P will be very small. The above condition can be satisfied and no temperature difference correction is needed. Further, the product of mass flow rate with the heat capacity of the cold and hot air is always approximately the same for the AHU heat exchanger, and the logarithmic mean temperature difference is almost equal to the arithmetic mean difference. All these conditions give us a reason to use the domain decomposition method for the thermal design of an AHU heat exchanger.

We propose the decomposition method of the thermal design (DMTD) as follows. For the cross-flow AHU heat exchanger shown in Fig. 11(a), the whole heat exchanger is divided into finite heat transfer cells along the direction of hot air flow direction and cold air flow direction. For the convenience of discussion, each direction is separated into four sections and a total of 16 cells are obtained as shown in Fig. 11(b). For every heat transfer cell, T_h(i,j) series and T_c(i,j) series are used to represent the average temperature of the inlet and outlet boundaries of every heat transfer cell. The inlet temperature of each cell is known, and the heat transfer rate and outlet temperature are unknown. To calculate the heat transfer rate in every cell, the following procedure is conducted:

First step: assuming a heat transfer rate dQ in the divided heat transfer cells.

Second step, calculating the outlet temperature of the (i,j) cell with the energy conservation equation:

$$T_{h\_out} = T_{h\_in} - \frac{dQ}{q_{m\_h} c_{p\_h}} \tag{2}$$

$$T_{c\_out} = T_{c\_in} + \frac{dQ}{q_{m\_c} c_{p\_c}} \tag{3}$$

where T_{h_in} and T_{h_out} are the inlet and outlet average temperature of the hot air respectively; T_{c_in} and T_{c_out} are the inlet and outlet average temperature of the cold air respectively; q_{m_h} and q_{m_c} are the mass flow rate of the hot air and cold air respectively; c_{p_h} and c_{p_c} are the heat capacity of the hot air and cold air respectively.

Third step: getting the arithmetic mean temperature difference ΔT with the T_{h_in}, T_{h_out}, T_{c_in}, and T_{c_out}:

$$\Delta T = \left(\frac{T_{h\_in}+T_{h\_out}}{2}\right) - \left(\frac{T_{c\_in}+T_{c\_out}}{2}\right) \tag{4}$$

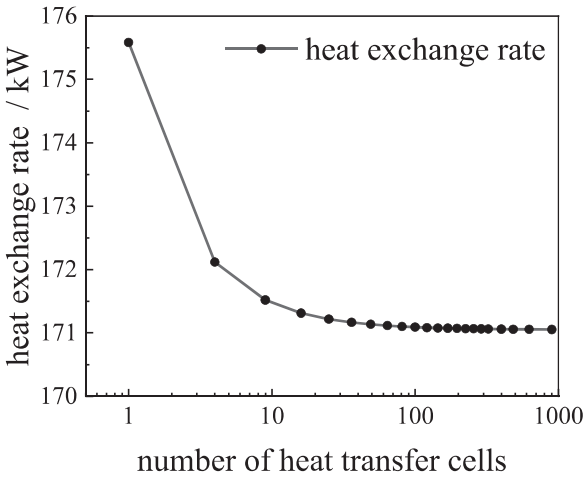

Fig. 12. Cell number independence test.

Then a "new heat transfer rate" dQ' is calculated according to the overall heat transfer equation:

$$dQ' = \frac{1}{\frac{1}{h_h A} + \frac{1}{h_c A}} \Delta T \tag{5}$$

where h_h and h_c are, respectively, the area-averaged convective heat transfer coefficient of the hot air and cold air. A is the projected area of the complex dimple/protrusion surface.

Fourth step: Correct the assumed heat transfer rate until the assumed and calculated ones are very close to each other. In the present paper, the relative error between two heat transfer rates is taken to less than 1×10^{-5}. For all cells, the heat exchange rate calculation starts from (0,0) cell and calculates in the first row from left to right, then calculates line by line form top to bottom until all cells are calculated.

To get the required finite cell number, an extreme case with the biggest h and heat transfer temperature difference as big as 32°C is used to calculate the relationship between the heat transfer rate and the number of cells. The results are shown in Fig. 12, where the abscissa for the cell number is in logarithm to clearly show the relationship of total heat rate versus cell number. 100 cells are enough to calculate the heat exchange rate of the whole heat exchanger. For the cases studied the deviation of the total heat transfer rate with 100 cells from the limiting case is only 0.02%.

It may be noted here that, in some sense, the proposed DMTD method is similar to the 1D flow network method (FNW). However, to the authors' knowledge, they are quite different. Taking reference [31] as an example where the FNW for the PEMFC is clearly presented, there are at least two major differences. First, all cells

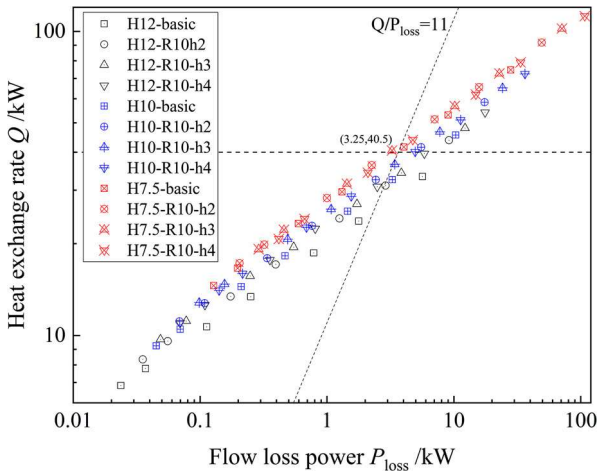

Fig. 13. Heat exchanger rate versus flow loss power plot of 12 channels.

are parallel to each other in the FNW, while in our DMTD method, one cell has two neighbors, one is its predecessor and the other is its successor. The three cells are connected in series, and several parallel series compose the hot or cold fluid flow route. Second, in the FNW all the cells are connected to the inlet manifold (from which every cell receives some flow rate) and outlet manifold (to which the cell flow rate goes), while in our DMTD method, the hot and cold flow are totally separated and heat transfer occurs between them.

4.2. The heat transfer and pressure drop estimation of designed heat exchangers

The following design conditions are assumed: 1. The hot air inlet temperature is 36°C, and the cold air inlet temperature is 15°C; 2. The heat exchanger rate (Q for short) is not less than 40 kW.

Based on the simulation data for the nine channels under different Reynolds numbers, the heat transfer rate and pressure drop can be calculated for the AHU heat exchangers assembled by the basic channels and nine enhanced channels. For the comparison among those heat exchangers under different flow rates, the total flow loss power of hot and cold air, denoted by P_{loss}, is calculated by Eq. (6).

$$P_{loss} = 2q_v\Delta p \tag{6}$$

where, P_{loss} is the flow loss power, kW. q_v is the air volume flow rate, and Δp is the pressure drop from the inlet surface to the outlet surface of the heat exchanger.

Applying the thermal design calculation method introduced in Section 4.1, the results shown in Fig. 13 are obtained. In the figure, the heat exchange rate versus P_{loss} is presented for all 12 AHU heat exchangers, and the abscissa for the P_{loss} and Q is in the logarithm.

The heat exchange rate of a heat exchanger is related to the heat transfer coefficient, the heat transfer area, and the heat transfer temperature difference. For all channels, with the increase of P_{loss}, the heat exchange rate increase trend gradually becomes mild. The reason is the decreasing heat transfer temperature difference when both air inlet temperature is fixed. In Fig. 13, on the whole, when P_{loss} is the same, the channels with smaller channel height will have a bigger heat exchange rate. The main reason is attributed to the increased heat transfer area.

The heat exchanger with the biggest heat exchange rate at the unit flow loss power within the nine enhanced channels is chosen to be the typical design result. According to the second design condition, the value of Q must be equal to or bigger than 40 kW. The most suitable heat exchanger is picked up by two dashed lines shown in Fig. 13. One is the horizontal line: $Q = 40$ kW; the other is the oblique line crossing the zero point and having the largest value of Q/P_{loss}. In Fig. 13, the point of "H7.5-R10-h3" (P_{loss} is 3.25 kW and Q is 40.5 kW) is picked as the typical design result, and this heat exchanger can guarantee the required heat exchange rate and the biggest ratio of Q over P_{loss} among all simulation cases.

4.3. Comparison of the proposed DMTD method with the CFD method/LTDM method

The proposed DMTD processes the advantages of both the CFD method and the LTDM while the disadvantages of the two methods are discarded. The CFD simulation results of the reasonable long simplified flow channels are adopted as the basic data of the DMTD process for calculating the heat transfer performance of the full-scale heat exchanger.

First, compared with the CFD method for designing an AHU, the computation time of DMTD is greatly saved while an accurate

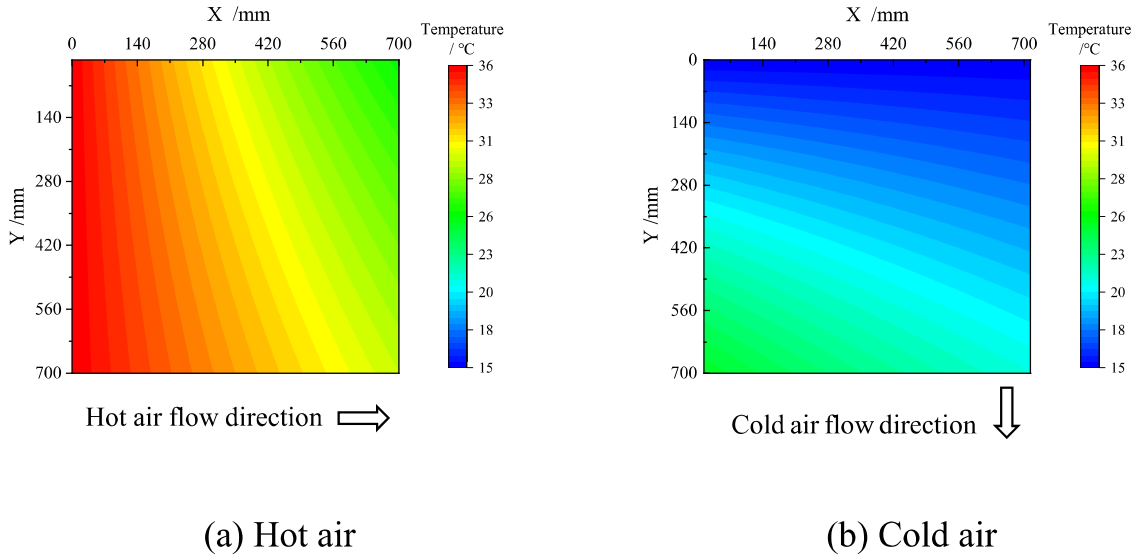

Fig. 14. Air temperature Contours of the hot air and cold air.

enough design result can be obtained. If only the CFD method is used to calculate the total heat transfer rate of the whole heat exchanger, the simulation domain will be at least the two adjacent channels as shown in Fig. 5. It is estimated that the mesh elements number will be larger than 900 million. A super computer is needed to finish the simulation at this mesh level. The DMTD method only needs 25.23 million mesh elements, it is obvious that the DMTD process requires much less computation time.

Second, compared with the LTDM method, the DMTD method is more convenient for engineering design which has been discussed in Section 4.1. And it can take the local variation of the air heat transfer coefficient (AHTE) into consideration. if the variation of the AHTE has been calculated based on long simulation channels in the design condition. Also, the LTDM method can only give the value of the heat exchange rate of the whole heat exchanger. The DMTD method can obtain the variation of the cross-section average temperature of the cold and hot air. As an example, Fig. 14 presented the temperature contours of the hot and cold air for the heat exchanger simulated by DMTD. The temperature contours could be used for further improvements at the local area of the heat exchanger where the heat transfer temperature difference becomes small.

5. Conclusion

The main conclusions of this paper are as follows:

1 The construction of the enhanced plate used in the AHU is proposed. On a given flat plate ECDs are firstly added to the fixed location, and then SCDs are applied to the flat surface among the ECDs.
2 The results of comprehensive numerical simulations within the Reynold number range from 5000 to 35,355 reveal that the Nusselt number increases appreciably with SCD depth and the effect of channel height is weaker than SCD depth. The SCD depth also has a stronger effect on f compared with channel height. For all enhanced channels, the PECs are larger than 1.1 within the studied Re range. The PEC at the low Reynold numbers range is higher than that at the high Reynolds number range. The performance of a deeper depth of SCD is superior to that of a shallow one when the channel height is the same. Among the nine channels studied, the highest enhanced effects are obtained for “H12-R10-h4” (PEC=1.45 at Re=5000).
3 By the performance evaluation method aimed at general energy saving effectiveness, it is found that all nine enhanced channels can enhance heat transfer at the same pressure drop. The energy saving performance decreases with Re, and the channels with smaller SCD depth can save more energy when channel height is fixed at the higher Reynolds number region.
4 The DMTD is proposed for the cross-flow AHU heat exchanger design. It possesses the advantages of both CFD and LTDM methods while discarding their disadvantages. It can provide the variation of the air cross-section average temperature and can take the local variation of heat transfer coefficient into consideration, and the computation time is acceptable for engineering design.
5 The proposed DMTD method is adopted to design AHUs with given inlet temperatures and heat transfer rates. Of eleven such designed heat exchangers, the one picked up is the “H7.5-R10-h3” which has the maximum ratio of the heat exchange rate (40.5 kW) over the flow loss power (3.25 kW).

Declaration of Competing Interest

The authors declare that they have no known competing financial interests or personal relationships that could have appeared to influence the work reported in this paper.

CRediT authorship contribution statement

Zixing Wang: Conceptualization, Methodology, Software, Validation, Formal analysis, Writing – original draft. **Hao Ding:** Software, Validation. **Le Lei:** Methodology. **Nan Li:** Methodology. **Wenquan Tao:** Resources, Writing – review & editing, Visualization, Supervision, Project administration, Funding acquisition.

Data availability

Data will be made available on request.

Acknowledgments

This work was supported by the Foundation for Innovative Research Groups of the National Natural Science Foundation of China [No. 51721004]; the Fund of Xi’an Science and Technology Bureau [2019218714SYS002CG024]; and the 111 Project [B16038].

References

[1] J. Niemann, J. Bean, V. Avelar, Economizer modes of data center cooling systems: Schneider Electric White, 2011, pp 3–4.
[2] U. Sajjad, N. Abbas, K. Hamid, et al., A review of recent advances in indirect evaporative cooling technology, Int. Commun. Heat Mass Transf. 122 (2021) 105140.
[3] Y.R. Min, Y. Chen, H.X. Yang, Numerical study on indirect evaporative coolers considering condensation: a thorough comparison between cross flow and counter flow, Int. J. Heat Mass Transf. 131 (2019) 472–486.
[4] A. Beghi, M. Lionello, M. Rampazzo, Efficient operation of indirect evaporative data center cooling systems via Newton-like extremum-seeking control, IEEE CCTA, Hong Kong, 2019, pp. 424–429.
[5] W.Y. Li, C.Y. Li, L.Y. Zeng, et al., Comparative study of vertical and horizontal indirect evaporative cooling heat recovery exchangers, Int. J. Heat Mass Transf. 124 (2018) 1245–1261.
[6] Q.L. Liu, C.M. Guo, Z.J. Wu, et al., Heat and mass transfer model optimization and annual energy efficiency analysis for energy recovery indirect evaporative cooling, Build. Simul. 15 (2022) 1353–1365.
[7] Y.D. Wan, Z.F. Huang, A. Soh, et al., Analysing the transport phenomena of novel dew-point evaporative coolers with different flow configurations considering condensation, Int. J. Heat Mass Transf. 170 (2021) 120991.
[8] S.D. Antonellis, L.C. Cignatta, C. Facchini, et al., Effect of heat exchanger plates geometry on performance of an indirect evaporative cooling system, Appl. Therm. Eng. 173 (2020) 115200.
[9] B. Zheng, C.M. Guo, T. Chen, et al., Development of an experimental validated model of cross-flow indirect evaporative cooler with condensation, Appl. Energy 252 (2019) 113438.
[10] S.D. Antonellis, C.M. Joppolo, P. Liberati, Performance measurement of a cross-flow indirect evaporative cooler: effect of water nozzles and airflows arrangement, Energy Build. 184 (2019) 114–121.
[11] S.S.M. Ajarostaghi, M. Zaboli, H. Javadi, et al., A review of recent passive heat transfer enhancement methods, Energies 15 (2022) 986.
[12] S. Rashidi, F. Hormozi, B. Sundén, et al., Energy saving in thermal energy systems using dimpled surface technology - a review on mechanisms and applications, Appl. Energy 250 (2019) 1491–1547.
[13] S. Shin, K.S. Lee, S.D. Park, et al., Measurement of the heat transfer coefficient in the dimpled channel: effects of dimple arrangement and channel height, J. Mech. Sci. Technol. 23 (2009) 624–630.
[14] G.N. Xie, J. Liu, P.M. Ligrani, et al., Numerical analysis of flow structure and heat transfer characteristics in square channels with different internal-protruded dimple geometrics, Int. J. Heat Mass Transf. 67 (2013) 81–97.
[15] Y.H. Xie, H.C. Qu, D. Zhang, Numerical investigation of flow and heat transfer in rectangular channel with teardrop dimple/protrusion, Int. J. Heat Mass Transf. 84 (2015) 486–496.
[16] J.S. Yang, M. Jeong, Y.G. Park, et al., Numerical study on the flow and heat transfer characteristics in a dimple cooling channel with a wedge-shaped vortex generator, Int. J. Heat Mass Transf. 136 (2019) 1064–1078.
[17] L. Zheng, Y.H. Xie, D. Zhang, Numerical investigation on heat transfer performance and flow characteristics in a rectangular air cooling channel (AR = 2) with ridged dimples, Int. J. Heat Mass Transf. 107 (2017) 403–417.
[18] A.I. Leontiev, N.A. Kiselev, Y.A. Vinogradov, et al., Experimental investigation of heat transfer and drag on surfaces coated with dimples of different shape, Int. J. Therm. Sci. 118 (2017) 152–167.
[19] M. Faizan, S.Z. Shuja, B.S. Yilbas, et al., Flow analysis of a rectangular channel with triangular and semi-spherical protrusions, Int. J. Therm. Sci. 162 (2021) 106793.
[20] E.M. Sparrow, J.M. Gorman, K.S. Friend, et al., Flow regime determination for finned heat exchanger surfaces with dimples/protrusions, Numer. Heat Transf. Part A Appl. 63 (2013) 245–256.

[21] J.F. Fan, W.K. Ding, Y.L. He, et al., Three-dimensional numerical study of fluid and heat transfer characteristics of dimpled fin surfaces, Numer. Heat Transf. Part A Appl. 62 (2012) 271–294.
[22] H. Zontul, H. Hamzah, N. Kurtulmuş, et al., Investigation of convective heat transfer and flow hydrodynamics in rectangular grooved channels, Int. Commun. Heat Mass Transf. 126 (2021) 105366.
[23] C. Chen, B.F. Bai, H.B. Wang, et al., Heat transfer enhancement of plate heat exchangers with symmetrically distributed capsules to generate counter-rotating vortices, Int. J. Heat Mass Transf. 151 (2020) 119455.
[24] C. Jiang, W.X. Zhou, X.Y. Tang, et al., Influence of capsule length and width on heat transfer in capsule-type plate heat exchangers, Adv. Mech. Eng. 11 (2019) 12.
[25] Y.F. Zhang, C. Jiang, Z.L. Yang, et al., Numerical study on heat transfer enhancement in capsule-type plate heat exchangers, Appl. Therm. Eng. 108 (2016) 1237–1242.
[26] Q. Jing, Y.H. Xie, D. Zhang, Numerical investigation of flow and heat transfer in rotating trapezoidal channel with lateral slots and dimple structure, Int. Commun. Heat Mass Transf. 118 (2020) 104865.
[27] J.F. Fan, W.K. Ding, J.F. Zhang, et al., A performance evaluation plot of enhanced heat transfer techniques oriented for energy-saving, Int. J. Heat Mass Transf. 52 (2009) 33–44.
[28] W.T. Ji, J.F. Fan, C.Y. Zhao, et al., A revised performance evaluation method for energy saving effectiveness of heat transfer enhancement techniques, Int. J. Heat Mass Transf. 138 (2019) 1142–1153.
[29] A.S. Tucker, The LMTD correction-factor for single pass crossflow heat exchangers with both fluids unmixed, ASME J Heat Transf. 118 (2) (1996) 488–490.
[30] W. Nusselt, Der Warmeubergang im Kreutzstrom, Z. Ver. deutsch. Ing. 55 (1911) 2021–2024.
[31] A. Amirfazli, S. Asghari, M. Sarraf, An investigation into the effect of manifold geometry on uniformity of temperature distribution in a PEMFC stack, Energy 145 (2018) 141–151.